Integrated Computer-Aided Engineering 17 (2010) 29–40
DOI 10.3233/ICA-2010-0327
IOS Press

An efficient fingerprint image compression technique based on wave atoms decomposition and multistage vector quantization

Abdul Adeel Mohammed , Rashid Minhas, Q.M. Jonathan Wu* and M.A. Sid-Ahmed
Computer Vision and Sensing Systems Laboratory, Department of Electrical Engineering, University of Windsor, Canada

Abstract. Modern fingerprint image compression and reconstruction standards used by the US Federal Bureau of Investigation (FBI) are based upon the popular biorthogonal 9-7 discrete wavelet transform. Multiresolution analysis tools have been successfully applied to fingerprint image compression for more than a decade; we propose a novel fingerprint image compression technique based on wave atoms decomposition and multistage vector quantization. Wave atoms decomposition has been specifically designed for enhanced representation of oscillatory patterns and to convey precise temporal and spatial information. Our proposed compression scheme is based upon multistage vector quantization of processed wave atoms representation of fingerprint images. Wave atoms expansion is processed using mathematical morphological operators to emphasize and retain significant coefficients for transmission. Quantized information is encoded using arithmetic entropy scheme. The proposed image compression standard outperforms other well established methods and achieves PSNR gain up to 8.07 dB in comparison to FBI's wavelet scalar quantization. Data mining, law enforcement, border security, and forensic applications can potentially benefit from our compression scheme.

Keywords: Image compression, fingerprint images, wave atoms decomposition, multistage vector quantization, arithmetic codings

1. Introduction

The fundamental goal of image compression is to obtain the best possible image quality at an allocated storage capacity. Law enforcement, border security and forensic applications are some crucial fields where fingerprint image compression plays an important role. Emergence of protocols and commercially available products has prompted law enforcement agencies to use Automated Fingerprint Identification Systems (AFIS) during criminal investigations. The US Federal Bureau of Investigation (FBI) deals with a massive collection of fingerprint database, containing more than 200 million cards, growing at the rate of 30,000–50,000 new cards daily [1]. The archive consists of inked impressions on paper cards. A single card contains 14 different images: 10 rolled impression of each finger, duplicate (flat) impression of thumb and simultaneous impression of all fingers together. Fingerprint images are digitized at a resolution of 500 pixels per inch with 256 gray levels which results into a fingerprint card requiring approximately 10 MB of storage. The gray level images tender a refined natural appearance to humans than black and white images and allow a higher level of subjective discrimination for fingerprint examiners. This investigation targets an efficient compression standard that can significantly reduce the image size while retaining distinctive information. In addition to the considerable

*Corresponding author: Computer Vision and Sensing Systems Laboratory, Department of Electrical Engineering, University of Windsor, ON, N9B3P4, Canada. E-mail: jwu@uwindsor.ca.

ISSN 1069-2509/10/$27.50

savings in memory, fingerprint image compression is also desired for effortless archiving and sweeping reduction in transmission bandwidth.

Fingerprint compression standard developed for FBI [3] has incorporated biorthogonal 9–7 filter pair for highly reliable fingerprint compression and reconstruction since 1993. Discrete Wavelet Transform (DWT) is a widely used mutliresolution analysis tool due to enhanced space-frequency decomposition of images [2], energy compaction of low frequency subbands, space localization of high frequency subbands and flexibility in time frequency tiling. Wavelet packets facilitate a flexible representation by allowing decompositions at every node of the tree resulting in an explicit structure for specific applications. Image analysis using DWT is performed using a pair of quadrature mirror filter (QMF) and a dual quadrature mirror filter (DQMF). These sets of filters are further decomposed into four subsets of floating point coefficients: h0(Lo_D), g0(Hi_D), h1(Lo_R) and g1(Hi_D) that define the wavelet and scaling functions for forward and inverse DWT respectively.

Fingerprint images are decomposed along their rows and columns using 2D DWT by means of separability approach resulting into four smaller subsets. Subsets are selected based on energy content, variance, their effect on reconstructed image, and are iteratively decomposed until desired number of subbands are obtained. These subbands are quantized and represented using different coding techniques. Researchers have proposed various techniques for iterative decomposition such as 64-subband [3] and 73-subband decomposition [4] methods. For improved subband decomposition Entropy Based Best Basis Selection (EBBBS) algorithm [5] has been proposed. Recently proposed fingerprint image compression schemes use genetic algorithm [6,7] to evolve wavelet and scaling coefficients for each level of decomposition.

In this paper we propose an efficient algorithm for fingerprint image compression using wave atoms decomposition. Extensive experiments are performed and the superior performance of our proposed multistage vector quantization based compression scheme is established against state-of-the-art algorithms. This paper is organized into 7 sections. Section 2 discusses the wave atoms transform along with its implementation details and Section 3 briefly explains the mathematical morphology operators followed by a discussion on multistage vector quantization in Section 4. The proposed method for fingerprint image compression is described in Section 5. Experimental results are discussed in Section 6 with remarks and conclusions briefed in Section 7.

2. Wave atoms decomposition

Fourier series decomposes a periodic function into a sum of simple oscillating functions, namely sines and cosines. In a Fourier series sparsity is destroyed due to discontinuities (Gibbs-like Phenomenon) and it requires a large number of terms to reconstruct a discontinuity precisely. Development of new mathematical and computational tools based on multiresolution analysis is a novel concept to overcome limitations of Fourier series. Many fields of contemporary science and technology benefit from multiscale, multiresolution analysis tools for maximum throughput, efficient resource utilization and accurate computations. Multiresolution tools render robust behavior to study information content of images and signals in the presence of noise and uncertainty.

Wavelet transform is a well known multiresolution analysis tool capable of conveying accurate temporal and spatial information. Wavelet transform has been profusely used to address problems in; signal and speech processing [32,33,62,67]; data compression [23–25,61], pattern recognition [27–29,31,34,36, 39,57,60], image reconstruction [55], and biomedical engineering applications [46,48,51,65]. Wavelets have ability to better represent objects with point singularities in 1D and 2D space but fail to deal with singularities along curves in 2D. Therefore wavelet representation does not offer sufficient sparseness for image analysis. Research community has witnessed intense efforts for development of new tools such as ridgelets [8], contourlets [9], and curvelets [10]. These tools have better directional and decomposition capabilities than wavelets.

Wave atoms are a recent addition to the collection of mathematical transforms for harmonic computational analysis. They are a variant of 2D wavelet packets that retain an isotropic aspect ratio, tender a sharp frequency localization that cannot be achieved using a filter bank based on wavelet packets and offer a significantly sparser expansion for oscillatory functions than wavelets, curvelets and Gabor atoms. Curvelets capture coherence only along oscillations whereas wave atoms capture coherence of pattern both along and across oscillations. Wave atoms precisely interpolate between Gabor atoms [14] (constant support) and directional wavelets [15] (wavelength is directly proportional to diameter) in the sense that the period of oscillations of each wave packet (wavelength) is related to the size of essential support by parabolic scaling i.e. wavelength is directly proportional to $(\text{diameter})^2$.

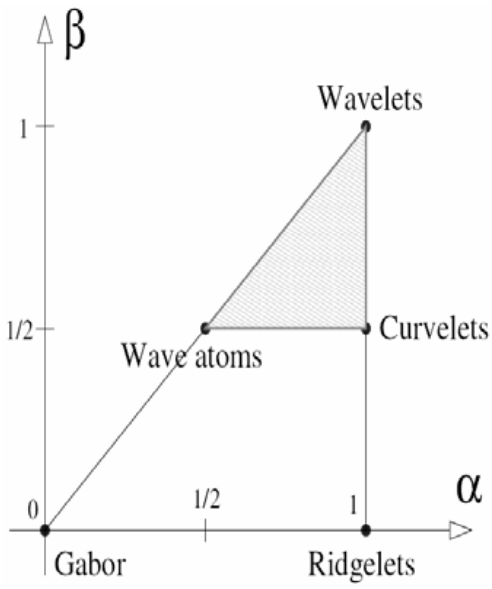

Fig. 1. Comparison of different wave packets architectures with respect to multiscale nature and directional selectivity [12].

Two distinct parameters α, β represent decomposition and directional ability and are sufficient for indexing all known forms of wave packet architectures namely wavelets, Gabor, ridgelets, curvelets and wave atoms. The triangle formed by wavelets, curvelets and wave atoms, as shown in the Fig. 1, indicates the wave packet families for which sparsity is preserved under transformation. Wave atoms are defined for $\alpha = \beta =$ 1/2, where α indexes the multiscale nature of the transform, from $\alpha =$ **0** (uniform) to $\alpha =$ **1** (dyadic). β measures the wave packet's directional selectivity (**0** and **1** indicate best and poor selectivity respectively). Wave atoms represent a class of wavelet packets where directionality is sacrificed at the expense of preserving sparsity of oscillatory patterns under smooth diffeomorphisms. Essential support of wave packet in space (left) and in frequency (right) is shown in Fig. 2.

2.1. 1D Discrete wave atoms decomposition

Wave atoms are constructed from tensor products of adequately chosen 1D wave packets. Let $\psi^j_{m,n}(x)$ represent a one-dimensional family of wave packets, where $j, m \geqslant 0$, and $n \in \mathbf{Z}$, centered in frequency around $\pm\omega_{j,m} = \pm\pi 2^j m$, with $C_1 2^j \leqslant m \leqslant C_2 2^j$ and centered in space around $x_{j,n} = 2^{-j}n$. One-dimensional version of the parabolic scaling states that the support of each bump of $\hat{\psi}^j_{m,n}(\omega)$ is of length $O(2^j)$ while $\omega_{j,m} = O(2^{2j})$. Dyadic scaled and translated versions of $\hat{\psi}^0_m$ in frequency domain are combined and the basis function is written as:

$$\psi^j_{m,n}(x) = \psi^j_m(x - 2^{-j}n) = 2^{j/2}\psi^0_m(2^j x - n). \quad (1)$$

The coefficients $c_{j,m,n}$, for each wave number $\omega_{j,m,n}$, are obtained as a decimated convolution at scale 2^{-j}.

$$c_{j,m,n} = \int \psi^j_m(x - 2^{-j}n)u(x)dx. \quad (2)$$

By Plancherel's theorem,

$$c_{j,m,n} = \int e^{i2^{-j}nw}\overline{\hat{\psi}^j_m(\omega)}\hat{u}(\omega)d\omega. \quad (3)$$

If the function u is discretized at, then with a small truncation error (3) is modified as:

$$c^D_{j,m,n} = \sum_{k=2\pi(-N/2+1:N/2)} e^{i2^{-j}nk}\overline{\hat{\psi}^j_m(k)}\hat{u}(k). \quad (4)$$

Since the data is supported inside two disjoint intervals of size $2^{j+1}\pi$, symmetric about origin (2^{j+1} points) instead of an interval of length 2^jx2π, sum(4) is computed using a reduced inverse FFT inside an interval of size $2^{j+1}\pi$ centered about origin:

$$c^D_{j,m,n} = \sum_{k=2\pi(-2^j/2+1:2^j/2)} e^{i2^{-j}nk} \sum_{p\in 2\,\pi Z} \overline{\hat{\psi}^j_m(k + 2^j p)}\hat{u}(k + 2^j p). \quad (5)$$

A simple wrapping technique is used for the implementation of discrete wavelet packets and the steps involved are:

1. Perform an FFT of size N on the samples of $u(k)$.
2. For each pair(j, m), wrap the product $\overline{\hat{\psi}^j_m}\hat{u}$ by periodicity inside the interval $[-2^j\pi, 2^j\pi]$ and perform an inverse FFT of size 2^j to obtain $c^D_{j,m,n}$.
3. Repeat step 2 for all pairs (j, m).

The overall complexity of the algorithm is *O* (*N LogN*) and the wavelet packets are decomposed into positive and negative frequency components, represented by

$$\hat{\psi}^j_{m,n}(\omega) = \hat{\psi}^j_{m,n,+}(\omega) + \hat{\psi}^j_{m,n,-}(\omega). \quad (6)$$

Hilbert transform $H\psi^j_{m,n}$ of Eq. (6) represents an orthonormal basis $L^2(R)$ and is obtained through a linear combination of negative and positive frequency bumps weighted by *i* and –*i* respectively.

$$H\hat{\psi}^j_{m,n}(\omega) = -i\hat{\psi}^j_{m,n,+}(\omega) + i\hat{\psi}^j_{m,n,-}(\omega). \quad (7)$$

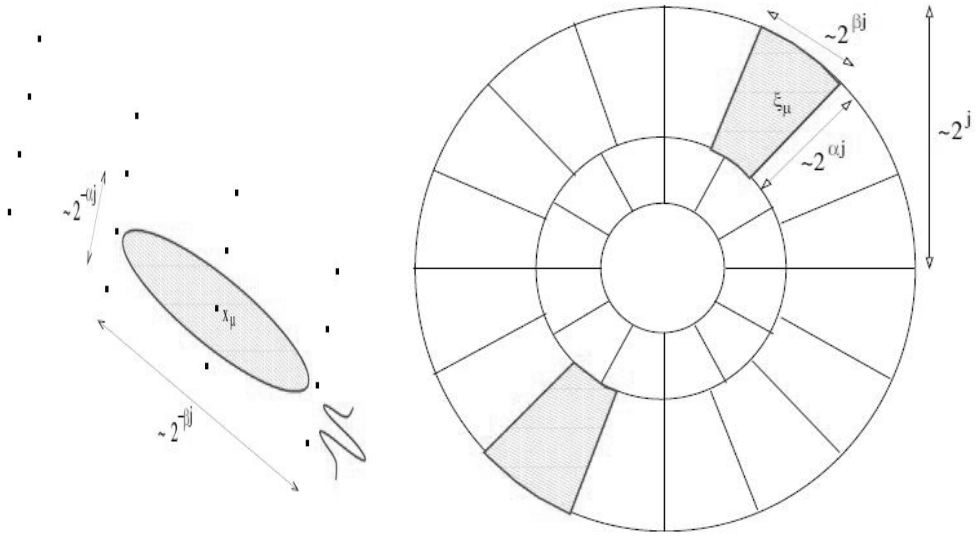

Fig. 2. Wave atoms tiling in space and frequency [12].

2.2. 2D discrete wave atoms

A two-dimensional orthonormal basis function with 4 bumps in frequency plane is formed by individually taking products of 1D wave packets. Mathematical formulation and implementations for 1D case are detailed in the previous section. 2D wave atoms are indexed by $\mu = (j, m, n)$, where $m = (m_1, m_2)$ and $n = (n_1, n_2)$. Construction is not a simple tensor product since there is only one scale subscript j. This is similar to the non-standard multi-resolution analysis wavelet bases where the point is to enforce same scale in both directions in order to retain an isotropic aspect ratio. Equation (1) is modified in 2D as:

$$\varphi_\mu^+(x_1, x_2) = \psi_{m1}^j(x_1 - 2^{-j}n_1) \psi_{m2}^j(x_2 - 2^{-j}n_2). \tag{8}$$

The Fourier transform of Eq. (8) is separable and its dual orthonormal basis is defined by Hilbert transformed wavelet packets in Eq. (10).

$$\hat{\varphi}_\mu^+(\omega_1, \omega_2) = \hat{\psi}_{m1}^j(\omega_1)e^{-i2^{-j}n_1\omega_1} \hat{\psi}_{m2}^j(\omega_2)e^{-i2^{-j}n_2\omega_2}. \tag{9}$$

$$\varphi_\mu^-(x_1, x_2) = H\psi_{m1}^j(x_1 - 2^{-j}n_1) H\psi_{m2}^j(x_2 - 2^{-j}n_2). \tag{10}$$

Combination of Eqs (8) and (10) provides basis functions with two bumps in the frequency plane, symmetric with respect to the origin and thus directional wave packets oscillating in a single direction are generated.

$$\varphi_\mu^{(1)} = \frac{\varphi_\mu^+ + \varphi_\mu^-}{2}, \varphi_\mu^{(2)} = \frac{\varphi_\mu^+ - \varphi_\mu^-}{2}. \tag{11}$$

$\varphi_\mu^{(1)}$ and $\varphi_\mu^{(2)}$ together form the wave atoms frame and are jointly denoted by φ_μ. Wave atoms algorithm is based on the apparent generalization of the 1D wrapping strategy to two dimensions and its complexity is $O(N^2 LogN)$.

3. Mathematical morphology operators

Mathematical morphology is the analysis of images in terms of their shape. It is used in image processing applications to preserve edge information and create clusters of significant coefficients [18]. The main building blocks of mathematical morphology are dilations and erosions. The basic effect of dilation on a binary image is to gradually enlarge the boundaries of regions of foreground pixels (i.e. white pixels, typically). Thus areas of foreground pixels grow in size while holes within those regions become smaller. Dilation of a binary input image is computed by superimposing the structuring element on top of the input image so that the origin of the structuring element coincides with the input pixel position. The input pixel is set to the foreground value if at least one pixel in the structuring element coincides with a foreground pixel in the image. If all the corresponding pixels in the image are background (black pixel i.e. 0), the input pixel is assigned as the background value. Erosion is the dual of dilation i.e. eroding foreground pixels is equivalent to

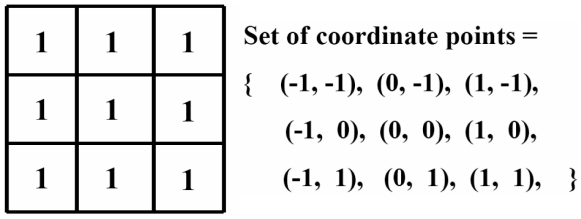

Fig. 3. A 3×3 square structuring element.

dilating the background pixels. Operations of dilation and erosion on an image X using a structuring element A are denoted by δ_A and ε_A respectively.

$$\delta_A(x) = X \oplus A \tag{12}$$

$$\varepsilon_A(x) = X \Theta A \tag{13}$$

To create clusters of significant coefficients we use mathematical morphology on significance map i.e. perform dilation twice followed by single erosion using a structuring element of size 3×3 as shown in Fig. 3. In this sequence of operations [19] the first dilation clusters the significant coefficient whereas the next dilation and erosion (also known as a closing operation) merely fill in small holes.

4. Multistage vector quantization

Vector Quantization (VQ) [20] is a quantization technique applied to an ordered set of symbols. The superiority of vector quantization lies in its ability to partition vector space, its capability to exploit intra-vector correlations and most importantly the block coding gain it achieves. MultiStage Vector Quantization (MSVQ) [21] divides the encoding stage into several smaller modules and reduces encoding complexity and memory requirements for vector quantization, especially at high compression ratios. In the first stage, a low rate vector quantizer is used to generate a relatively crude encoding of the input vector using a small codebook. The coarse approximation in the form of output labels of the vector quantizer is transmitted to the receiver. The error between the original input and the coarse representation of the first stage is quantized by the second stage quantizer and the label of the output point is transmitted to the receiver. Similarly the input to the N^{th} stage vector quantizer is the difference between the original input and the reconstruction obtained from the preceding $N-1$ stages.

In vector quantization, an input vector is quantized by selecting the best matching representation from amongst a codebook of *2kr* stored code vectors each of dimension k. Vector quantization is an optimal coding technique since other coding methods for a specified number $b = kr$ of bits are equivalent to special cases of VQ with suboptimal codebooks. However, optimal VQ assumes single and possibly very large codebook with no imposed constraints in its structure. The resulting encoding and storage complexity, of the order of *2kr*, may be prohibitive for many applications. Multistage vector quantization is a structured VQ scheme that can achieve very low encoding and storage complexity. In MSVQ, the *kr* bits are divided between N stages with b_i bits for stage i. The storage complexity of MSVQ is $\sum_{i=1}^{N} 2^{b_i}$ vectors, significantly less than the complexity of $\prod_{i=1}^{N} 2^{b_i} = 2^{kr}$ vectors required for an unstructured VQ. A sequential quantization operation is performed in MSVQ where each stage quantizes the residual of the previous stage. The structure of MSVQ encoder [21] consists of a cascade of VQ stages as shown in Fig. 4. For an N-stage MSVQ, each n^{th}stage quantizer Q_n, $n = 1, 2, \ldots, N$ is associated with a stage codebook C_n that contains K_n stage code vectors. The set of stage quantizers $Q_1, Q_2, \ldots, Q_N$ are equivalent to a single quantizer Q, referred as the direct-sum vector quantizer.

In the MSVQ encoder shown in Fig. 4, the input vector X, is quantized with the first stage codebook producing the first stage code vector $Q_1(X)$, a residual vector is formed by subtracting $Q_1(X)$ from X. Then residual vector is quantized using the second stage codebook, with exactly the same procedure as in the first stage. Therefore in each stage except the last stage, a residual vector is generated and passed to the next stage to be quantized independently of other stages. The quantized error vector provides a refinement to the previous vector quantizer output and the level of correlation decreases as the process continues.

$$\begin{aligned} Y_1 &= Q_1(X). \\ Y_2 &= Q_2(X - Q_1(X)). \\ Y_3 &= Q_3(X - Q_1(X) - Q_2(X - Q_1(X))). \end{aligned} \tag{14}$$

The block diagram of an MSVQ decoder is shown in Fig. 5, for each stage the decoder receives an output label identifying the stage code vector selected and the reconstruction vector $\hat{X}$ is generated as:

$$\hat{X} = Y_1 + Y_2 + Y_3. \tag{15}$$

The overall quantization error is equal to the quantization residual from the last stage. Sequential searching of the stage codebooks reduces the encoding complexity to the storage complexity i.e. $\sum_{i=1}^{N} 2^{b_i}$.

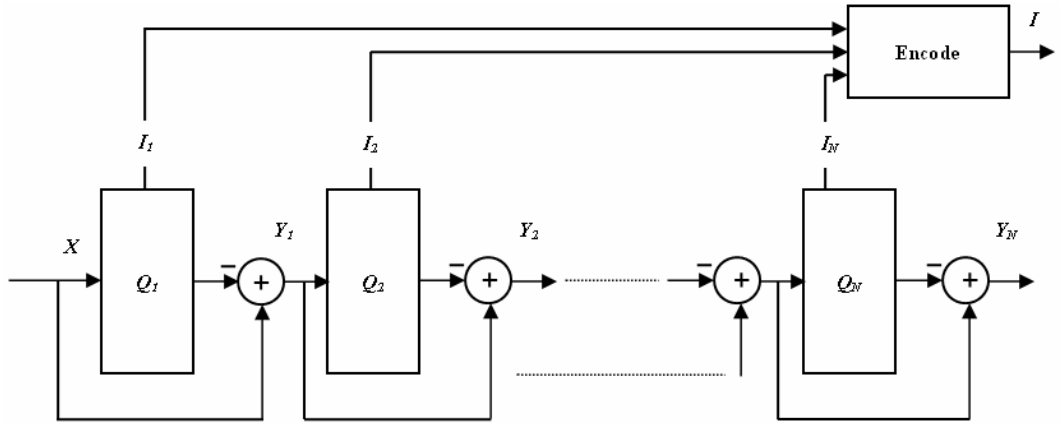

Fig. 4. Block diagram of an MSVQ encoder.

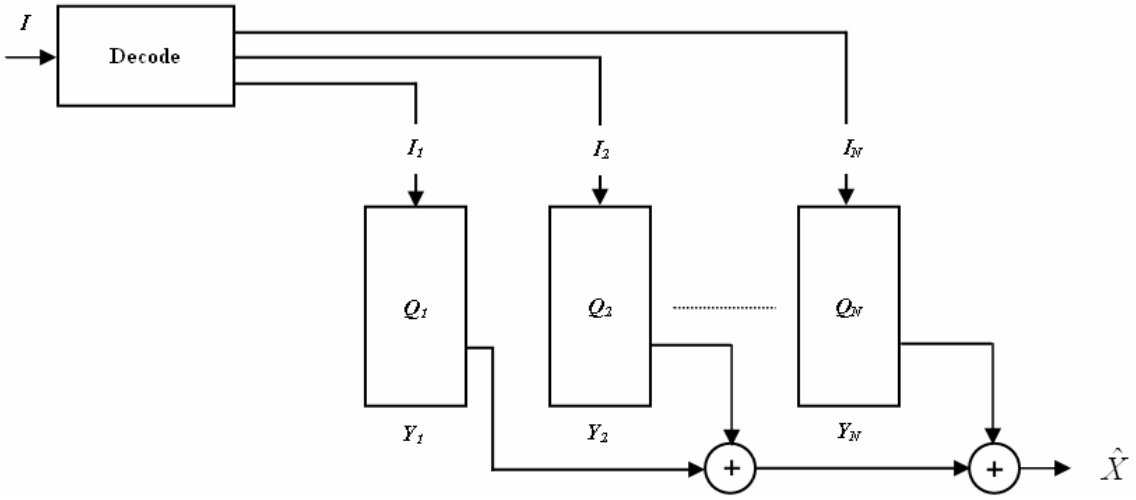

Fig. 5. Block diagram of an MSVQ decoder.

5. Proposed algorithm

Our proposed algorithm is based on an innovative multiresolution analysis tool termed as wave atoms decomposition and is an extension of our earlier work [22]. Important steps involved in our proposed scheme are depicted in Fig. 6; we do not assume any *a priori* information and acquisition constraints for the input data. Fingerprint images are digitized using 256 gray levels therefore a transformation in color space is not required. To retain fine details in an image no further pre-processing, contrast enhancement and filtering operations are performed. Wave atoms decomposition is used for sparse representation and detection of coherence patterns of fingerprints since they belong to the category of images that oscillate smoothly in varying directions. Discrete 2D wave atoms decomposition is applied on the original fingerprint images to efficiently capture coherence patterns along and across the oscillations. An orthonormal basis $\varphi_{\mu}^{+}(x)$ $(\varphi_{\mu}^{(1)} + \varphi_{\mu}^{(2)})$ is used instead of a tight frame since each basis function oscillates in two distinct directions instead of one. This orthobasis variant property is significantly important in applications where redundancy is undesired.

To achieve efficient compression, image data with low information content such as smooth areas can be represented using fewer numbers of coefficients. The magnitudes of wave atoms decomposed coefficients, carrying low information content, are either zero or very close to zero hence they can be discarded without a substantial degradation in reconstructed image quality. An appropriate global threshold is used to define each coefficient as either significant or not and this threshold

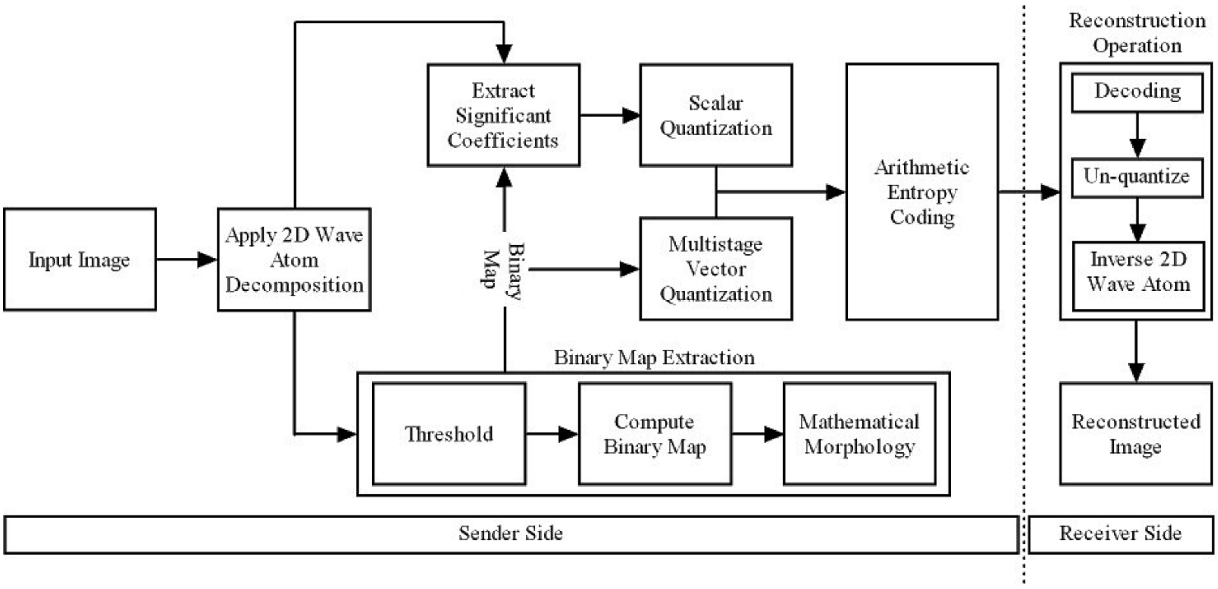

Fig. 6. Block diagram of the proposed compression algorithm.

is defined according to the user's need, and represents a tradeoff between quality and compression; a small threshold results in better reconstructed image quality with lower compression whereas a larger threshold attains reconstructed images with poor quality at high compression ratio. The thresholding operation generates a significance binary map whose values are selected as '1' if the magnitude of wave atoms decomposed coefficient is greater than a predefined threshold at that location and '0' otherwise. In significance map, values of '1' and '0' indicate the presence or absence of significant coefficient at a specific location. Please note that the size of significance map is similar to the dimension of the coefficients obtained after wave atoms decomposition. To corroborate improved image reconstruction, we apply morphological operators on significance map to be used at later stage for extraction and quantization of actual coefficients. The mathematical morphology procedure comprises of dilations and erosions to minimize the loss of potentially important coefficients because of thresholding thereby ensuring a high peak signal to noise ratio of the reconstructed image. The AND operation among significance map and original wave atoms decomposed coefficients is used to extract coefficients carrying important and discriminative information of oscillatory patterns in an input image. Such extracted coefficients, termed as significant coefficients, are scalar quantized using a uniform scalar quantizer with 512 distinct levels.

Blocks of p $\times$ p elements of the significance map are non-uniformly vector quantized using a MSVQ (please see Section 4 for details). The quantization process tries to eliminate psycho-visual redundancy which causes degradation in image quality. Additional loss of coefficient information is attributed to thresholding. In our proposed method the significance map is divided into non-overlapping blocks of 4 $\times$ 4 elements and vectorized into small length vectors of dimension 16 $\times$ 1; small blocks of data are used in order to minimize error during vector quantization. These vectors are quantized using MSVQ scheme resulting into a codebook representation termed as MSVQ quantized significance map.

The scalar quantized significant coefficients and MSVQ quantized significance map are transformed using an arithmetic encoder. Arithmetic coding is a variable length entropy scheme that attempts to minimize the number of bits by converting a string into another representation using more bits for infrequent characters and *vice versa*. As opposed to other encoding techniques which convert the input message into the component symbols and replace each symbol with a code word; arithmetic coding represents the entire message into a single number thereby achieving optimal entropy encoding. For a communication setup, the computation of encoded information using entropy scheme is a last step at the senders end before information is being transferred whereas decoding, un-quantization and inverse 2D wave atoms decomposition are applied to reconstruct the transformed image.

Table 1
PSNR VALUES AT DIFFERENT COMPRESSION RATIOS

CR	Bit rate	FBI's WSQ [3] PSNR (dB)	Compression with VQ [22] PSNR (dB)	Proposed PSNR (dB)
80	0.1	23.72	28.62	29.98
53.3	0.15	25.15	29.06	30.53
40	0.2	26.25	31.21	33.23
32	0.25	27.14	31.52	34.84
26.6	0.3	27.96	31.68	35.78
22.8	0.35	28.72	32.36	36.07
20	0.4	29.36	32.42	36.59
17.7	0.45	29.89	32.47	37.38
16	0.5	30.37	32.65	38.44

6. Experiments

Various fingerprint images are compressed using the proposed method and substantial improvement in results is achieved. The quality of various image compression techniques depends upon how close is the reconstructed image to the original image. Different quality measures have been proposed to evaluate the quality of compression algorithms, some methods investigate similarity while others explore the level of dissimilarity between reconstructed and the reference image.

Mean Square Error (MSE) and Peak Signal to Noise Ratio (PSNR) are two notable metrics used to examine the qualitative performance. Mean square error is a distortion metric that provides a measure of dissimilarity between two images, whereas PSNR represents a ratio of maximum possible power of a signal and the power of the corrupting noise/distortion that affects the fidelity of its representation.

$$MSE = \frac{1}{R * C} \sum_{i=1}^{R} \sum_{j=1}^{C} |I_o(i,j) - I_r(i,j)|^2, \quad (16)$$

$$PSNR = 10 \log_{10} \frac{255^2}{MSE}, \quad (17)$$

where R indicates the number of image rows and C refers to the number of columns, $I_o(,)$ represents the original image whereas $I_r(,d)$ refers to the reconstructed image.

A sample fingerprint image used in evaluating the performance of the proposed compression algorithm is shown in Fig. 7(a). Compressed images at a Compression Ratio (CR) of 12.9 using FBI's Wavelet Scalar Quantization (WSQ), VQ on wave atoms decomposition and the proposed MSVQ based wave atoms scheme are shown in Figs. 7(b-d) respectively. It is evident from Fig. 7(d) that the proposed method using wave atoms decomposition performs better in preserving the fine details in a fingerprint image (i.e. the minutiae – ridges ending and bifurcations) and contains less blur in comparison with FBI's WSQ standard and VQ based wave atoms decomposition.

Table 1 compares the PSNR values obtained using our proposed method, for different compression ratios, against various methods. As shown in Table I, fingerprint compression based on wave atoms decomposition and multistage vector quantization produces a significant improvement in PSNR at high compression ratios (low bit rates). We compare the performance of our proposed MSVQ based compression standard with WSQ [3] and our earlier work [22]. In [22], we developed a compression scheme based on linear vector quantization of decomposed wave atoms representation of fingerprint images; wave atoms decomposed coefficients were thresholded and a significance map matrix and a significant coefficient vector generated. The significance map was divided into non-overlapping blocks, vectorized and quantized using K-means vector quantization scheme with 64 code words. Results are compared at higher compression since most standards perform reasonably well at lower compression rates but their performance drastically deteriorates at higher values. At a compression ratio of 19:1, genetic algorithm based multiresolution analysis algorithm [17] achieves a maximum MSE improvement of 16.71% and a PSNR gain of 0.794 dB over the FBI fingerprint compression standard. However our proposed algorithm offers a maximum PSNR gain of 8.07 dB at a compression ratio of 16:1 compared to WSQ.

Additional experiments are performed to establish the improved performance of our proposed method against state-of-the-art schemes. Two publicly available fingerprint images, whorl and tented arch type [56], are used and compared against contourlets [54] for varying combinations of filter banks. The subjective evaluations for achieved compression using wave atoms decomposition for tented arch and whorl type images are presented in Fig. 8. It is clearly evident that the recon-

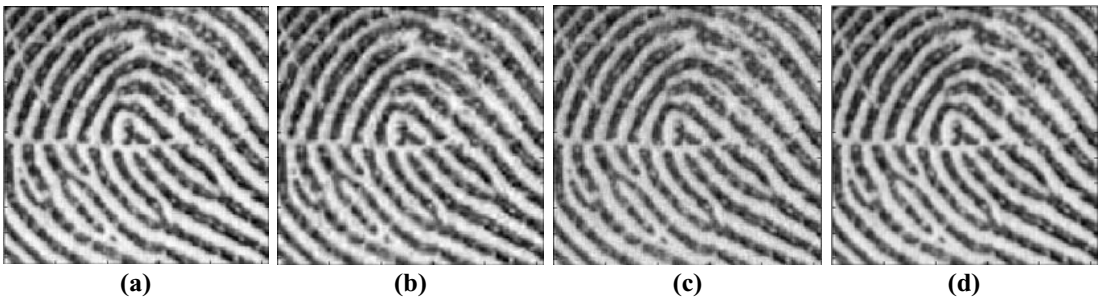

Fig. 7. Performance comparison of various methods at CR = 12.9:1. (a) original fingerprint image (b) compressed image using FBI's WSQ (c) compressed image using wave atoms decomposition and VQ (d) compressed image using proposed method.

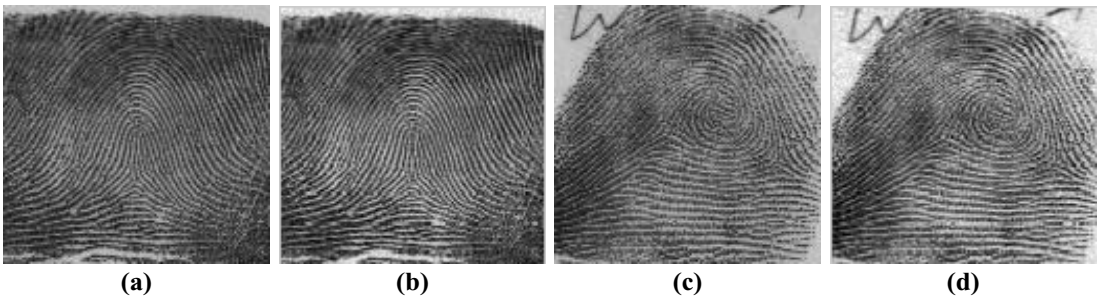

Fig. 8. Original and reconstructed images using our proposed method (a-b) original and reconstructed tented arch type image (c-d) original and reconstructed whorl type image.

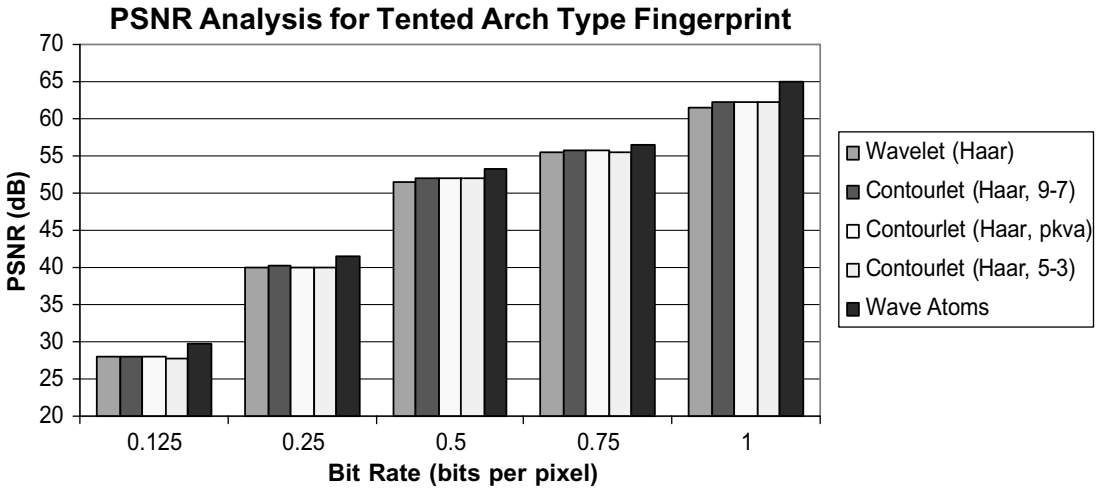

Fig. 9. PSNR analysis for various methods using tented arch type fingerprint image.

structed images at a rate of 1 bit per pixel have close resemblance with the source images along with all the minute details being precisely preserved.

For fair analysis we compared PSNR values obtained for various methods as presented in Figs 9–10. Please be reminded that the PSNR improvements for both sets of images, i.e. whorl and tented arch, are quite similar thus the analyses for only tented arch type fingerprint image are presented. The methods used for performance analysis against our proposed scheme include Haar wavelets, contourlets based on varying combinations of Pyramidal and Directional filter banks (5-3, 9-7, Haar and pkva). It is clear that the PSNR values for compression based on wave atoms decomposi-

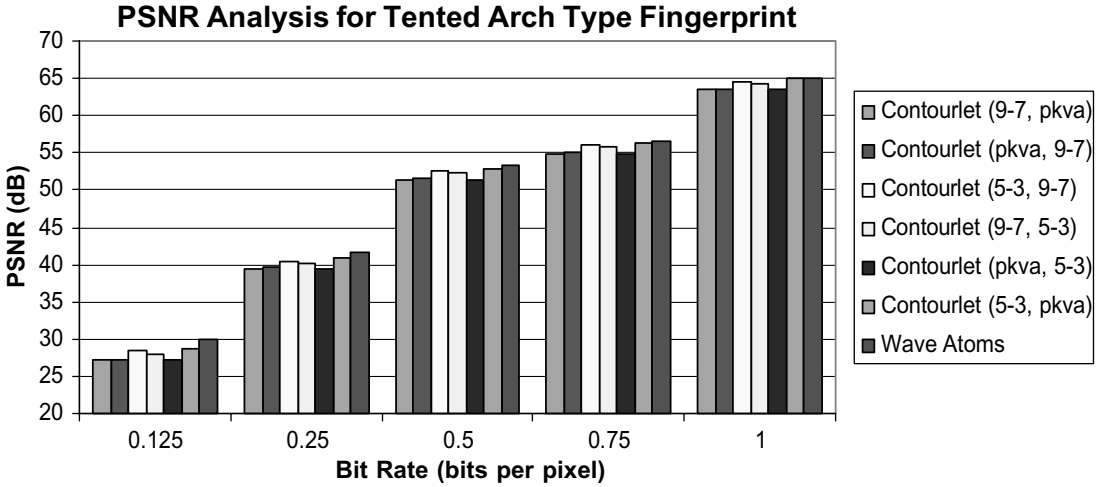

Fig. 10. PSNR analysis for various methods using tented arch type fingerprint image.

tion is monotonically increasing and consistently higher against other methods for rising compression rates. From Fig. 9, it is noticeable that the performance of Haar wavelets and contourlets is analogous however none of these methods visibly outperform the other.

7. Conclusion

Application of mathematical morphology and MSVQ to numerous fingerprint images generates an improved PSNR for a specified compression ratio. Multistage vector quantization efficiently represents the significance map using fewer bits and radically improves PSNR values. The performance of proposed wave atoms decomposition based multistage vector quantizer is significantly better in terms of PSNR compared against well established standards. The improvements in PSNR are more pronounced and distinct at higher compression ratios and achieve PSNR gain up to 8.07 dB against FBI's WSQ. Experimental results validate the fact that wave atoms decomposition supports sparser expansion, for oscillatory functions, than wavelets, and contourlets. Improvements in PSNR are greatly attributed to wave atoms that capture coherence of pattern both across and along oscillations. In future we would like to exploit dependency amongst wave atoms coefficients at various scales and orientations which may facilitate automated threshold computation for improved compression.

Acknowledgement

The work is supported in part by the Canada Research Chair program, the Natural Sciences and Engineering Research Council of Canada Discovery Grant and AUTO21 NCE. Authors would also like to extend gratitude to waveatom.org team for useful links and data.

References

[1] C.N. Brislawn, J.N. Bradley, R. Onyshczak and T. Hopper, The FBI Compression Standard for Digitized Fingerprint Images, *In Proceedings of SPIE* **2847** (1996), 344–355.

[2] R.A. DeVore, B. Jawerth and B. Lucier, Image Compression through Wavelet Transforms Coding, *In IEEE Transactions on Information Theory* **38** (1992), 719–746.

[3] J.N. Bradley and C.N. Brislawn, Proposed First Generation WSQ Bit Allocation Procedure, *In Proceedings of Criminal Justice Information Servies Technology* (1993), C11–C17.

[4] S. Kasaei, M. Deriche and B. Boashash, Fingerprint Compression Using a Modified Wavelet Transform and Pyramid Lattice Vector Quantization, *In IEEE Proceedings of TENCON* **2** (1996), 798–803.

[5] R.R. Coifman and M.V. Wickerhauser, Entropy Based Algorithm for Best Basis Selection, *In IEEE Transactions on Information Therory* **38** (1992), 713–718.

[6] U. Grasemann and R. Mikkulainen, Evolving Wavelets Using a Coevolutionary Genetic Algorithm and Lifting, *In Proceedings of Sixth Genetic and Evolution Computation Conference* (2004), 969–980.

[7] F. Moore, Evolved Multi-resolution Analysis Transforms for Optimized Image Compression and Reconstruction under Quantization, *In WSEAS Transactions on Computers* **1** (2006), 97–104.

[8] M.N. Do and M. Vetterli, The Finite Ridgelet Transform for Image Representation, *In IEEE Transactions on Image Processing* **12** (2003), 16–28.

[9] M.N. Do and M. Vetterli, The Contourlet Transform: An Efficient Directional Multiresolution Image Representation, *In IEEE Transactions on Image Processing* **14** (2005), 2091–2106.
[10] E.J. Candès, L. Demanet, D.L. Donoho and L. Ying, Fast Discrete Curvelet Transforms, *In Multiscale Modeling and Simulation* (2005), 861–899.
[11] L. Villemoes, Wavelet Packets with Uniform Time-Frequency Localization, *In Comptes Rendus Mathematique* **335** (2002), 793–796.
[12] L. Demanet and L. Ying, Wave Atoms and Sparsity of Oscillatory Patterns, *Appl Comput Harmon Anal* **23** (2007), 368–387.
[13] L. Demanet and L. Ying, Scattering in Flatland: Efficient Representations via Wave Atoms, *In Foundation of Computational Mathematics*, 2008.
[14] S. Mallat, A Wavelet Tour of Signal Processing *Second Edition, Academic Press*, Orlando-SanDiego, 1999.
[15] J.P. Antoine and R. Murenzi, Two-dimensional Directional Wavelets and the Scale-Angle Representation, *In Signal Processing* **52** (1996), 259–281.
[16] L. Demanet and L. Ying, Curvelet and Wave Atoms for mirror extended images, *In Proceedings of SPIE* **6701** (2007), 6701–6719.
[17] B. Babb and F.Y. Moore, The Best Fingerprint Compression Standard Yet, *In Proceedings of IEEE Systems, Mann and Cybernetics* (2007), 2911–2916.
[18] J. Serra, Image Analysis and Mathematical Morphology, *Academic Press*, New York, 1988.
[19] E. Morales and F. Shih, Wavelet coefficients clustering using morphological operations and pruned quadtree, *In IEEE Transactions on Pattern Recognition* **10** (2000), 1611–1620.
[20] Y. Linde, A. Buzo and R.M. Gray, An algorithm for vector quantizer design, *In IEEE Transactions on Communication* **28** (1980), 84–95.
[21] H. Khalil and K. Rose, Multistage vector quantizer optimization for packet networks, *In IEEE Transactions on Signal Processing* **51** (2003), 1870–1879.
[22] A.A. Mohammed, R. Minhas, Q.W.J. Wu and M.A. Sid-Ahmed, A generic fingerprint image compression technique based on wave atoms decomposition, *In Proceedings of IEEE Interntional Conference on Image Processing*, 2009.
[23] H. Adeli and A. Karim, A Fuzzy-Wavelet RBF Neural Network Model for Freeway Incident Detection, *Journal of Transportation Engineering*, ASCE, **126**(6) (2000), 464–471.
[24] H. Adeli and A. Samant, An Adaptive Conjugate Gradient Neural Network – Wavelet Model for Traffic Incident Detection, *Computer-Aided Civil and Infrastructure Engineering* **13**(4) (2000), 251–260.
[25] A. Samant and H. Adeli, Feature Extraction for Traffic Incident Detection using Wavelet Transform and Linear Discriminant Analysis, *Computer-Aided Civil and Infrastructure Engineering* **13**(4) (2000), 241–250.
[26] A. Samant and H. Adeli, Enhancing Neural Network Incident Detection Algorithms using Wavelets, *Computer-Aided Civil and Infrastructure Engineering* **16**(4) (2001), 239–245.
[27] A. Karim and H. Adeli, Comparison of the Fuzzy – Wavelet RBFNN Freeway Incident Detection Model with the California Algorithm, *Journal of Transportation Engineering*, ASCE, **128**(1) (2002), 21–30.
[28] A. Karim and H. Adeli, Incident Detection Algorithm Using Wavelet Energy Representation of Traffic Patterns, *Journal of Transportation Engineering*, ASCE, **128**(3) (2002), 232–242.
[29] A. Karim and H. Adeli, Fast Automatic Incident Detection on Urban and Rural Freeways Using the Wavelet Energy Algorithm, *Journal of Transportation Engineering*, ASCE, **129**(1) (2003), 57–68.
[30] H. Adeli, Z. Zhou and N. Dadmehr, Analysis of EEG Records in an Epileptic Patient Using Wavelet Transform, *Journal of Neuroscience Methods* **123**(1) (2003), 69–87.
[31] S. Ghosh-Dastidar and H. Adeli, Wavelet-Clustering-Neural Network Model for Freeway Incident Detection, *Computer-Aided Civil and Infrastructure Engineering* **18**(5) (2003), 325–338.
[32] Z. Zhou and H. Adeli, Time-frequency signal analysis of earthquake records using Mexican hat wavelets, *Computer-Aided Civil and Infrastructure Engineering* **18**(5) (2003), 379–389.
[33] Z. Zhou and H. Adeli, Wavelet Energy Spectrum for Time-Frequency Localization of Earthquake Energy, *International Journal of Imaging Systems and Technology* **13**(2) (2003), 133–140.
[34] H. Adeli and S. Ghosh-Dastidar, Mesoscopic-Wavelet Freeway Work Zone Flow and Congestion Feature Extraction Model, *Journal of Transportation Engineering*, ASCE, **130**(1) (2004), 94–103.
[35] H. Adeli and H. Kim, Wavelet-Hybrid Feedback Least Mean Square Algorithm for Robust Control of Structures, *Journal of Structural Engineering*, ASCE, **130**(1) (2004), 128–137.
[36] X. Jiang and H. Adeli, Wavelet Packet-Autocorrelation Function Method for Traffic Flow Pattern Analysis, *Computer-Aided Civil and Infrastructure Engineering* **19**(5) (2004), 324–337.
[37] H. Kim and H. Adeli, Hybrid Control of Smart Structures Using a Novel Wavelet-Based Algorithm, *Computer-Aided Civil and Infrastructure Engineering* **20**(1) (2005), 7–22.
[38] H. Kim and H. Adeli, Wavelet Hybrid Feedback-LMS Algorithm for Robust Control of Cable-Stayed Bridges, *Journal of Bridge Engineering*, ASCE, **10**(2) (2005), 116–123.
[39] X. Jiang and H. Adeli, Dynamic Wavelet Neural Network for Nonlinear Identification of Highrise Buildings, *Computer-Aided Civil and Infrastructure Engineering* **20**(5) (2005), 316–330.
[40] H. Kim and H. Adeli, Hybrid Control of Irregular Steel Highrise Building Structures Under Seismic Excitations, *International Journal for Numerical Methods in Engineering* **63**(12) (2005), 1757–1774.
[41] X. Jiang and H. Adeli, Dynamic Wavelet Neural Network Model for Traffic Flow Forecasting, *Journal of Transportation Engineering*, ASCE, **131**(10) (2005), 771–779.
[42] H. Kim and H. Adeli, Wind-Induced Motion Control of 76-Story Benchmark Building Using the Hybrid Damper-Tuned Liquid Column Damper System, *Journal of Structural Engineering*, ASCE, **131**(12) (2005), 1794–1802.
[43] H. Adeli and X. Jiang, Dynamic Fuzzy Wavelet Neural Network Model for Structural System Identification, *Journal of Structural Engineering*, ASCE, **132**(1) (2006), 102–111.
[44] S. Ghosh-Dastidar and H. Adeli, Neural Network-Wavelet Micro-Simulation Model for Delay and Queue Length Estimation at Freeway Work Zones, *Journal of Transportation Engineering*, ASCE, **132**(4) (2006), 331–341.
[45] X. Jiang, S. Mahadevan and H. Adeli, Bayesian Wavelet Packet Denoising for Structural System Identification, *Structural Control and Health Monitoring* **14**(2) (2007), 333–356.
[46] H. Adeli, S. Ghosh-Dastidar and N. Dadmehr, A Wavelet-Chaos Methodology for Analysis of EEGs and EEG Subbands to detect Seizure and Epilepsy, *IEEE Transactions on Biomedical Engineering* **54**(2) (2007), 205–211.
[47] X. Jiang and H. Adeli, Pseudospectra, MUSIC, and Dynamic Wavelet Neural Network for Damage Detection of Highrise

Buildings, *International Journal for Numerical Methods in Engineering* **71**(5) (2007), 606–629.
[48] S. Ghosh-Dastidar, H. Adeli and N. Dadmehr, Mixed-band Wavelet-Chaos-Neural Network Methodology for Epilepsy and Epileptic Seizure Detection, *IEEE Transactions on Biomedical Engineering* **54**(9) (2007), 1545–1551.
[49] X. Jiang and H. Adeli, Dynamic Fuzzy Wavelet Neuroemulator for Nonlinear Control of Irregular Highrise Building Structures, *International Journal for Numerical Methods in Engineering* **74**(7) (2008), 1045–1066.
[50] X. Jiang and H. Adeli, Neuro-Genetic Algorithm for Nonlinear Active Control of Highrise Buildings, *International Journal for Numerical Methods in Engineering* **75**(8) (2008), 770–786.
[51] H. Adeli, S. Ghosh-Dastidar and N. Dadmehr, A Spatio-temporal Wavelet-Chaos Methodology for EEG-based Diagnosis of Alzheimer's Disease, *Neuroscience Letters* **444**(2) (2008), 190–194.
[52] M. Figueroa-Villanueva, N.K. Ratha and R.M. Bolle, A Comparative Performance Analysis of JPEG 2000 vs. WSQ for Fingerprint Image Compression, *Lecture Notes in Computer Science* **2688** (2003), 385–392.
[53] A.K. Al-Asmari, Progressive edge detection compression for fingerprint images, *International Journal of Imaging Systems and Technology* **12**(5) (2003), 211–216.
[54] S. Esakkirajan, T. Veerakumar, V. Murugan and R. Sudhakar, Fingerprint Compression Using Contourlet Transform and Multistage Vector Quantization, *International Journal of Biological and Medical Sciences* **1**(2) (2006), 140–147.
[55] M. Rizzi, M. D'Aloia and B. Castagnolo, Computer Aided Detection of Microcalcifications in Digital Mammograms Adopting a Wavelet Decomposition, *Integrated Computer-Aided Engineering* **16**(2) (2009), 91–103.
[56] http://biometrics.cse.msu.edu/fingerprint.html.
[57] W.C. Yau, D.K. Kumar and S.P. Arjunan, *Visual Recognition of Speech Consonants using Facial Movement Features* **14**(1) (2007), 49–61.
[58] H. Lee, E. Kim and M. Park, A genetic feature weighting scheme for pattern recognition, *Integrated Computer-Aided Engineering* **14**(2) (2007), 161–171.
[59] I. Villaverde, M. Grana and A. d'Anjou, Morphological Neural Networks and Vision Based Simultaneous Localization and Mapping, *Integrated Computer-Aided Engineering* **14**(4) (2007), 355–363.
[60] Q. Wu and J. Ben-Arie View Invariant Head Recognition by Hybrid PCA based Reconstruction, *Integrated Computer-Aided Engineering* **15**(2) (2008), 97–108.
[61] I. Zyout, I. Abdel-Qader and H. Al-Otum, Progressive Lossy to Lossless Compression of ROI in Mammograms: Effects on Microcalcification Detection, *Integrated Computer-Aided Engineering* **15**(3) (2008), 241–251.
[62] M. Walid, W. Saleh and A.B. Hamadou, A Hybrid Approach for Automatic Lip Localization and Viseme Classification to Enhance Visual Speech Recognition, *Integrated Computer-Aided Engineering* **15**(3) (2009), 253–266.
[63] D.T. Lin and D.C. Pan, Integrating a Mixed-Feature Model and Multiclass Support Vector Machine for Facial Expression Recognition, *Integrated Computer-Aided Engineering* **16**(1) (2009), 61–74.
[64] J.C. Noyer, P. Lanvin and M. Benjelloun, Correlation-based particle filter for 3D object tracking, *Integrated Computer-Aided Engineering* **16**(2) (2009), 165–177.
[65] S. Ghosh-Dastidar and H. Adeli, Improved Spiking Neural Networks for EEG Classification and Epilepsy and Seizure Detection, *Integrated Computer-Aided Engineering* **14**(3) (2007), 187–212.
[66] K. Raftopoulos, N. Papadakis, K. Ntalianis and S. Kollias, Shape-based Invariant Classification of Gray Scale Images, *Integrated Computer-Aided Engineering* **14**(4) (2007), 365–378.
[67] I. Luican, H. Zhu and F. Balasa, Computation of the Minimum Data Storage and Applications in Memory Management for Multimedia Signal Processing, *Integrated Computer-Aided Engineering* **15**(2) (2008), 181–196.
[68] R.T.K. Lin, J.L. Chiu, H. Dai, R.T. Tsai, M. Day and W. Hsu, A Supervised Learning Approach to Biological Question Answering, *Integrated Computer-Aided Engineering* **16**(3) (2009), 271–281.